Journal of Polymer Research (2020) 27: 14
https://doi.org/10.1007/s10965-019-1981-4

ORIGINAL PAPER

Poly(1,6-heptadiyne)/ABS functionalized microfibers for hydrophobic applications

Pawan Kumar[1] · Prakash M. Gore[2] · RaviPrakash Magisetty[2] · Balasubramanian Kandasubramanian[2] · Raja Shunmugam[1]

Received: 16 April 2019 / Accepted: 20 November 2019 / Published online: 11 December 2019

Abstract

We report an electrospun & thermally stable micro-fibers of poly(1,6-heptadiyne) (PHD), modified with ABS. Developed micro-fibers demonstrated hydrophobicity (WCA~145° ± 2°), and exhibited hierarchical surface morphology (confirmed by FESEM analysis). Simulation study showed Chi parameter i.e. $\chi_c = 7.88$, & free energy of mixing i.e. 4.67 kcal/mol, thereby demonstrating its feasibility for electrospinning. PHD/ABS microfibers demonstrated low ice-adhesion ability, where, it effectively removed frozen water droplets in 8 s from hydrophobic surface, under an air-stream rate of 78 kPa/s. High thermal stability (200 °C), hydrophobicity and low ice-adhesion ability, demonstrate that PHD/ABS microfibers can be effectively used for multifunctional engineering/industrial applications.

Keywords Poly(1,6-heptadiyne) (PHD) · Acrylonitrile butadiene styrene (ABS) · Micro-fibers · Hydrophobic · High temperature · Electrospinning

Introduction

The rising need of materials exhibiting intrinsic controlled surface wettability [1] & high temperature service durability under severe environmental conditions has inspired & accelerated the development of hydrophobic & superhydrophobic materials [2–4] for multifunctional engineering & industrial applications such as wearable electronics, self-cleaning textiles & coatings [5, 6], thermo-switchable wetting surfaces [7, 8], anti-biofouling surfaces [9], icephobic materials [7], cleaning of contaminated water [10–13], and oil-water separation [14–17], etc. For rendering a controlled wettability in materials by means of hydrophobic-hydrophilic/oleophobic-oleophilic surface attributes, it is necessary to engineer and enhance surface roughness (at micro−/nano scale), along with reduced surface energy [14, 15]. Various methodologies and techniques have been employed for the fabrication of materials exhibiting engineered surface architectures such as wax solidification [18], lithography [19], chemical vapor deposition [20], templating method [21], sol-gel method [22], electrodeposition [23], Layer-by-Layer [24], One-pot reaction [25], controlled-combustion method [26, 27], polymer modification/conformation [28], electrospinning [14, 15] etc. Among these methods, electrospinning is an efficient processing technique which facilitates high surface area to volume ratio, material combination and mass production compatibility, processability and low cost, thus making it attractive for various industrial applications e.g. hydrophobic and wearable electronics, etc.

Considering various reported polymers exhibiting functionality, few researchers have explored thermoset polymers for hydrophobic surface applications [29–33]. Shang et al., have described a fabrication of a thermoset based nanofibrous membrane composed of cellulose acetate (CA) nanofibers (300~500 nm) and fluorine functionalized polybenzoxazine (F-PBZ) (in-situ polymerized) functional layer engineered with silica nanoparticles (SiO_2) (30~70 nm). This F-PBZ/

Electronic supplementary material The online version of this article (https://doi.org/10.1007/s10965-019-1981-4) contains supplementary material, which is available to authorized users.

✉ Balasubramanian Kandasubramanian
meetkbs@gmail.com

✉ Raja Shunmugam
polyraja@gmail.com

[1] Department of Chemical Sciences, Indian Institute of Science Education & Research, Kolkata, Mohanpur 741 246, India

[2] Nano Surface Texturing Lab, Department of Metallurgical & Materials Engineering, Defence Institute of Advanced Technology (DU), Ministry of Defence, Girinagar, Pune 411025, India

SiO_2 and cellulose acetate based nanofibrous membrane exhibited a superhydrophobicity (WCA~161°) and superoleophilicity (OCA~3°) along with surface roughness of 4.10 μm [34]. PHD, which is a thermoset based polymer, is least explored for hydrophobic applications [35, 36], being thermally stable up to 400 °C with a high glass transition temperature (Tg) of more than 300 °C coupled with excellent optical transparency, low moisture absorption, low birefringence [32], and a low dielectric constant [37–39]. PHD and its various derivatives [40–44] find their use & applications, ranging from optical polymers, in flat panel displays and waveguides [45, 46] drug delivery system, dielectric encapsulants for electronic packaging, oil spill management and sacrificial materials for microelectromechanical systems (MEMS) [47, 48]. Although, PHD and its derivatives are utilized in various engineering applications [40–45, 48–50], mechanical brittleness, and low adhesiveness, inhibit the applications of PHD to some extent. Yet researchers have not explored the viability of PHD engineered nano−/micro-fibers for hydrophobic applications involving thermal stability [14, 15].

In this context, we report 1–6-heptadiynes engineered with ABS micro-fibers, by employing solution blending and fabricated via facile electrospinning technique. The developed PHD/ABS micro-fibers possess a porous nonwoven structure and hierarchical textured morphology as confirmed by the FE-SEM analysis. The PHD derivatives and ABS exhibit a high thermal stability i.e. T_m~400 °C & T_g~300 °C for PHD derivatives, and T_m~230 °C & T_g~112 °C for ABS thermoplastic [24]. The miscibility study of the PHD derivatives & ABS polymer i.e. Chi parameter (χ_c) & free energy mixing, were computed by employing molecular dynamics simulation analysis via Accelrys Materials Studio software (Supporting Information). The hydrophobicity of the developed porous nonwoven micro-fibers is evaluated using static contact angle method and has been explained using the Wenzel & Cassie-Baxter regimes. The PHD/ABS engineered porous nonwoven micro-fibers also demonstrated a low ice adhesion ability, where it effectively detached frozen water droplets in 8 s under an air pressure of 78 kPa. Considering the successive enhanced results and higher intrinsic properties, we propose to use the developed PHD/ABS blended fibrous structures for engineering and industrial applications, where hydrophobic surfaces exhibiting high temperature stability are essentially required.

Materials and methods

Materials

ABS terpolymer (Absolac 920) was procured from Styrolution ABS India Ltd., which exhibited melt flow rate of 27 g/10 min at 220 °C, and density ~ 1.04 g/cc. PHD polymer (Mw~2500 g/mol) powder in its purified form was kindly supplied by Indian Institutes of Science Education and Research, Kolkata, India and further studies were done at Defence Institute of Advanced Technology, India. Ethyl acetate & Dichloromethane (DCM) were procured from Sigma-Aldrich, India.

Methods

Synthesis of monomer Diacetylene (DA)

Propargyl functionalized malonic ester, monomer diacetylene (DA) was synthesized by our previously reported literature.[52] For the formation of DA, malonic ester was treated with sodium hydride in presence of dry THF under inert condition at 0 °C. Then propargyl bromide was added dropwise and kept to stir for 36 h at room temperature. Then reaction mixture was washed with ethyl acetate and water. Organic layer collected and dried to get crude product. Compound was purified using column chromatography method with 5% of eluent of ethyl acetate and hexane. After column chromatography light yellow compound was collected, this was further recrystallizing to get pure solid compound with 90% yield. Formation of compound was further confirms by different spectroscopies techniques. In ^{1}H NMR spectroscopy, peaks at δ ppm 2.05 and 2.90 corresponds to acetylene moiety and peaks at δ ppm 4.2 and 1.2 corresponds to ester group confirms the formation DA. (Fig. 1a) Formation of DA was confirmed by ^{13}C and FT-IR spectroscopies. (Figure S3)

Synthesis of poly(1,6-heptadiynes), PHD

DA was taken under inert condition and dissolve in dry THF. Then catalytic amount of Hoveyda Grubbs' second generation catalyst was added and kept to stir for 2 h at room temperature 45, 52, 53]. Reaction was quenched by ethyl vinyl ether and then solvent was dried. Then obtained product was precipitated with diethyl ether. Then the precipitated product was dried under vacuum. Formation of PHD was confirmed by ^{1}H NMR spectroscopies and APC analysis. In ^{1}H NMR spectroscopy, absence of peaks at δ 2.05 corresponds to acetylene group and new peaks at δ ppm 4.80 and 5.75 confirms the formation of PHD polymer. (Figure S4) Then APC analysis was done using THF as eluent and polymethylmethacrylate as standards to check the molecular weight of polymer PHD, which was found as Mn = 2500 g / mol with polydispersity index, = 1.30 (Fig. 1b).

Synthesized PHD polymer exhibits conjugation in structure, which brings it a red-orange colour. Therefore, UV-vis study was done and absorbance study was done with different concentrations in chloroform (Fig. 2a). Then, 1 mg of PHD was dissolved in 10 ml of HPLC-THF and morphological analysis was done using FESEM. The morphological analysis showed rod-like structure (diameter~55 nm) for PHD polymer (Fig. 2b).

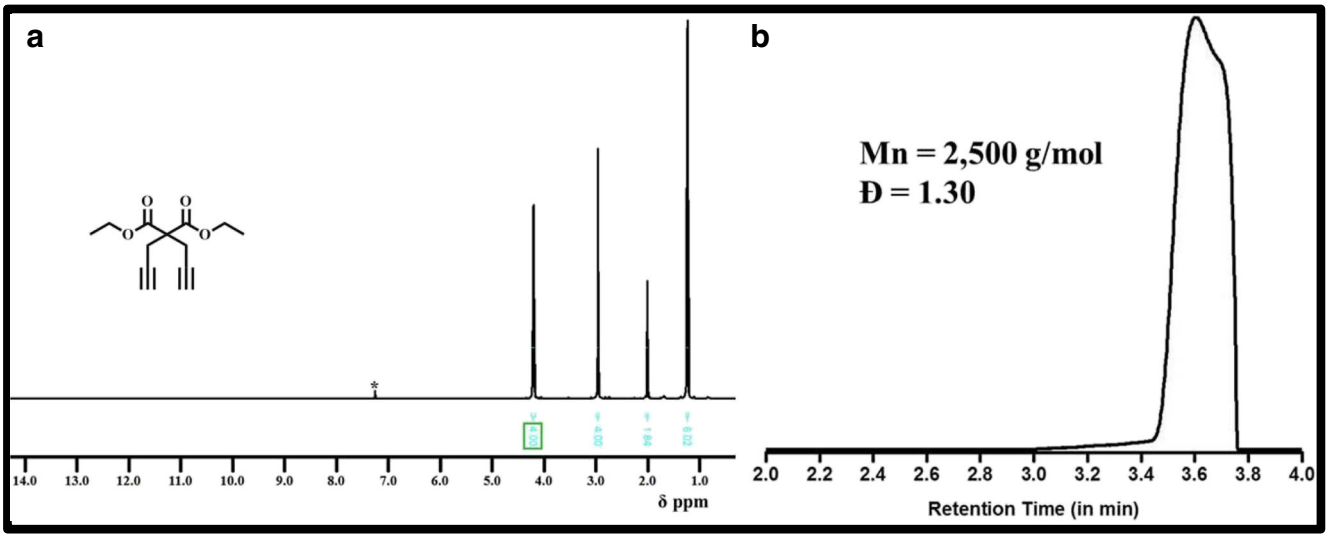

Fig. 1 **a** ^{1}H-NMR of compound **Diacetylene** in $CDCl_3$, **b** GPC of compound PHD

Fiber processing methods

Considering the functional advantages, electrospinning method was chosen for the fabrication of PHD/ABS nanofibers **(**Table 1**).** The comparison and advantages electrospinning method are provided below.

Large surface area to volume ratio: The nano-scale of electrospun fibers facilitate it a large surface area.
Wide range of materials: Considering the targeted applications e.g. biomedical or electronics, of nanofibers, various compatible materials based on polymers and ceramics can be employed for electrospinning.
Nanofiber functionalization: Functionalization of nanofibers be accomplished through simple solution blending before and after spinning, and/−or co-electrospinning setup.
Deposition of nanofibers on substrates: Nanofibers can be deposited on various polymeric, metallic, and ceramic substrates.
Bulk production ability: The nanofibers can be produced on large scale by using number of needles, or by employing needleless electrospinning method. [49, 51].

Methodology of electrospinning

Separate homogeneously dispersed solutions of ABS 30% (wt/v) & ABS-PHD blend were prepared using Dichloromethane (DCM) as solvent, under magnetic stirring (300 rpm) for 60 mins at room temperature, as per the method reported in our recent literature [49]. Weight percent loading of PHD in ABS solution was kept at 0.1, 0.2, 0.3, and

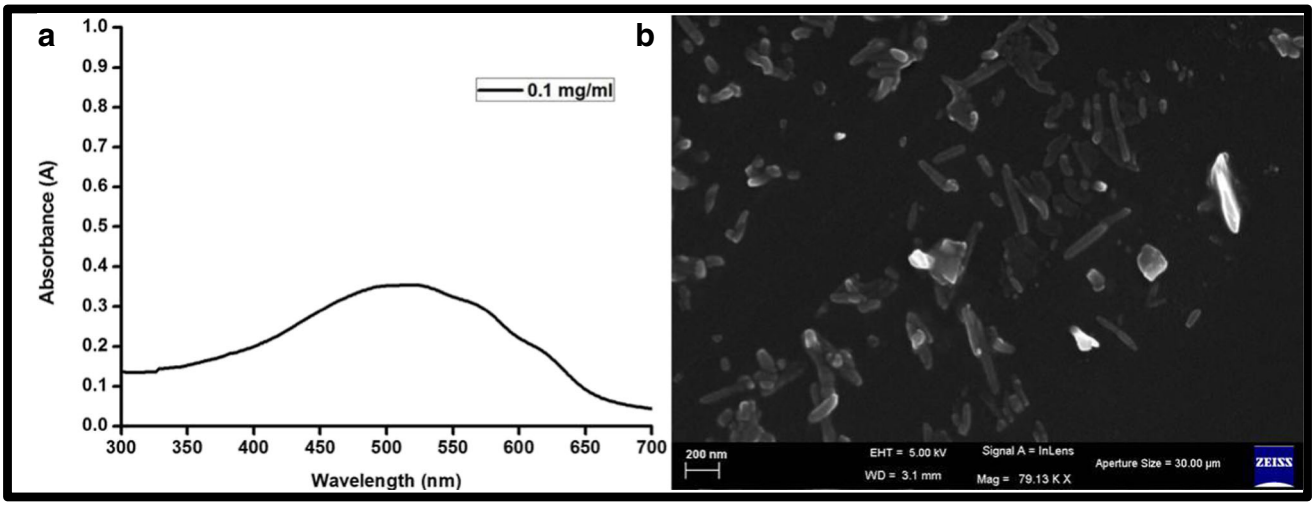

Fig. 2 **a** UV-vis study of PHD polymer, **b** FE-SEM analysis of PHD polymer

Table 1 Fiber production methods

Fabrication Techniques	Advantages	Disadvantages	Ref.
Temperature-induced phase separation Method	Modest equipment	Restricted to specific polymers, Non scalable, Poor control on fiber morphology.	[49, 51]
Drawing	Modest equipment	Non scalable, Intermittent process, Poor control on fiber morphology.	
Molecular self-assembly	Restricted to fabrication of nanofibers of few nanometer in diameter and few micrometer in length	Intricate process, Non scalable, Poor control on fiber morphology	
Template synthesis	Continuous process, Fiber morphology can be varied using various techniques	Not scalable	
Electrospinning	Modest instrument, Cost effective, Continuous method, scalable, fiber dimensions can be controlled	Instability of jet, hazard of noxious solvents, handling	

0.4 wt%. DCM is a volatile & polar solvent, thus, it helps in rendering the required electrical conductivity to the solution, and faster drying of generated microfibers, during electrospinning operation [49]. These, homogeneously dispersed solutions were utilized for electrospinning operation for the generating the microfibers, as illustrated in Fig. 3. During electrospinning operation, needle tip to collector plate distance was maintained at 12 cm, voltage was maintained at 15 kV, along with a solution feed rate of 3 μL/min, at room temperature.

Pre-measurement of solution viscosity helps in adjusting the electrospinning parameters during generation of microfibers. During electrospinning operation, needle tip to collector plate distance was maintained at 12 cm, voltage was maintained in the range of 15 kV, along with a solution feed rate of 3 μL/min.

Characterization techniques

Molecular weight and its distribution (dispersity index (Đ)) of synthesized polymeric product were analyzed using GPC method (Make: Waters Acquity). ^{1}H NMR spectroscopy was performed Bruker (Model: 500 MHz) and Jeol (Model:400 MHz) spectrometers by using $CDCl_3$ as solvent. UV-visible absorption was carried out with the aid of UV-Vis spectroscopy PerkinElmer Lambda 35. Wettability of generated PHD/ABS micro-fibers was characterized using the static water contact angle goniometer (DSA 25, Kruss GmbH, Germany), using deionized water with 8 μl volume of the droplet at room temperature. Solution viscosity was measured using Brookfield viscometer (DVII Pro, Brookfield Engineering Laboratories Inc., USA) using a spindle no. 21, and a rotational speed of 10 rpm, shear rate of 0.166/s, at room temperature. Molecular dynamics simulations were performed using Accelrys Materials Studio software via Blends module and polymer consistent force-field (Supporting Information).

Results & discussion

Morphological analysis

Morphological study was performed for exploring the hierarchical nano−/micro surface texture of engineered PHD/ABS micro-fibers as shown in Fig. 4. FE-SEM micro-graphs reveal surface micro-texture of the developed PHD-ABS micro-fibers. In Fig. 4a and e, progressive surface texture of the microfibers is observed. At Fig. 4a and b of Pristine ABS &

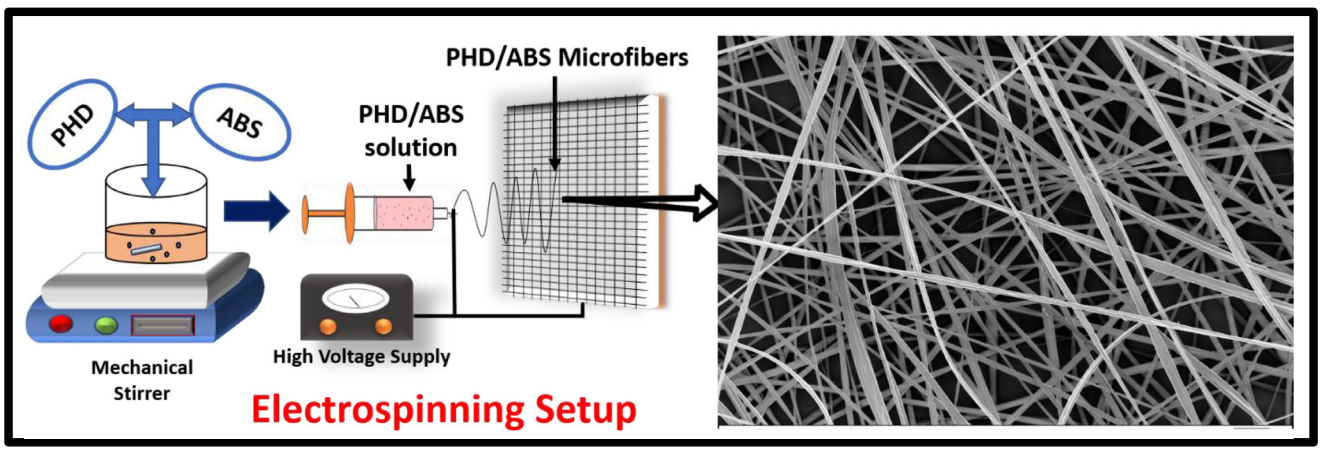

Fig. 3 Pictorial representation of electrospinning of PHD/ABS micro-fibers

0.1 PHD/ABS micro-fibers respectively, it is observed that the micro-fiber diameter is non-uniform and irregularly patterned. Figure 4c-e, show the uniform micro-fiber diameter with improved surface-microtexture, which is attributed to the respective increased concentration of PHD polymer in PHD/ABS micro-fibers. PHD polymer & PHD/ABS blend doesn't possess a polar or functional group in the backbone or side chains (except acrylonitrile group in the ABS side chain), which in turn might be reducing the Van der Wall forces leads to reducing adhesion between two phases & improving the hydrophobic nature of the developed micro-fibers [37, 49, 50, 52].

FESEM micrographs as shown in Fig. 5a–e, reveal nano-scaled surface texture & morphology of the pristine ABS and PHD/ABS micro-fibers. Figure 5b–e, reveal a phase separated morphology of the PHD/ABS micro-fibers, which could be attributed to immiscible nature of PHD & ABS homopolymers in the blend system (also confirmed by the molecular dynamics simulations analysis) [53, 54], which separate out during the electrospinning process, where a high voltage charge causes the blend solution to be melt stretched along the length of the micro-fibers, thereby exhibiting a phase separated morphology in the erstwhile immiscible homopolymers. The average fiber diameters for pristine ABS & PHD/ABS micro-fibers were found to be 2.87 ± 1.11 μm & 3.2 ± 1.15 μm, respectively (measured using SPIP 6.7.7 Image Metrology software). The difference in the diameters of the electrospun pristine ABS & PHD/ABS micro-fibers is also attributed to the phase separated morphology of PHD & ABS homopolymers, which causes the increment in micro-fibers diameter. Micro-fibers clearly show a porous structure with an average pore diameter of 152 ± 78 nm (measured using SPIP 6.7.7 Image Metrology software), along the length of microfibers, as shown in Fig. 5d. The generation of pores in the micro-fibers is attributed to the evaporation of DCM solvent during the drying process, where the entrapped solvent molecules under the action of drying temperature try to escape from the microfibers, thereby making the hollow pores in the micro-fibers [52].

The histograms were plotted for the distribution of the pores i.e. voids, in the developed nanofibers, which is shown in Fig. 6. The study of histograms revealed that the Pristine ABS microfibers exhibited pores having an average size of 51 ± 37.76 μm^2, 0.1 wt% PHD-ABS microfibers showed pores having an average size of 122.85 ± 79 μm^2, 0.2 wt% PHD-ABS microfibers exhibited pores having an average size of 74.92 ± 40.61 μm^2, 0.1 wt% PHD-ABS microfibers showed pores having an average size of 60 ± 37.36 μm^2, and 0.4 wt% PHD-ABS microfibers exhibited pores having an average size of 98.26 ± 70.47 μm^2.

Wettability analysis

The wettability behavior of the PHD/ABS micro-fibers was evaluated using the static contact angle method. The pristine ABS micro-fibers possessed hydrophobicity (WCA~137° ± 2°) **(**Fig. 7**),** whereas static water contact angles for the 0.2, 0.3, and 0.4 wt% PHD/ABS micro-fibers were found to be 139° ± 2°, 142° ± 1.6° and 145° ± 2°, respectively [54]. Water

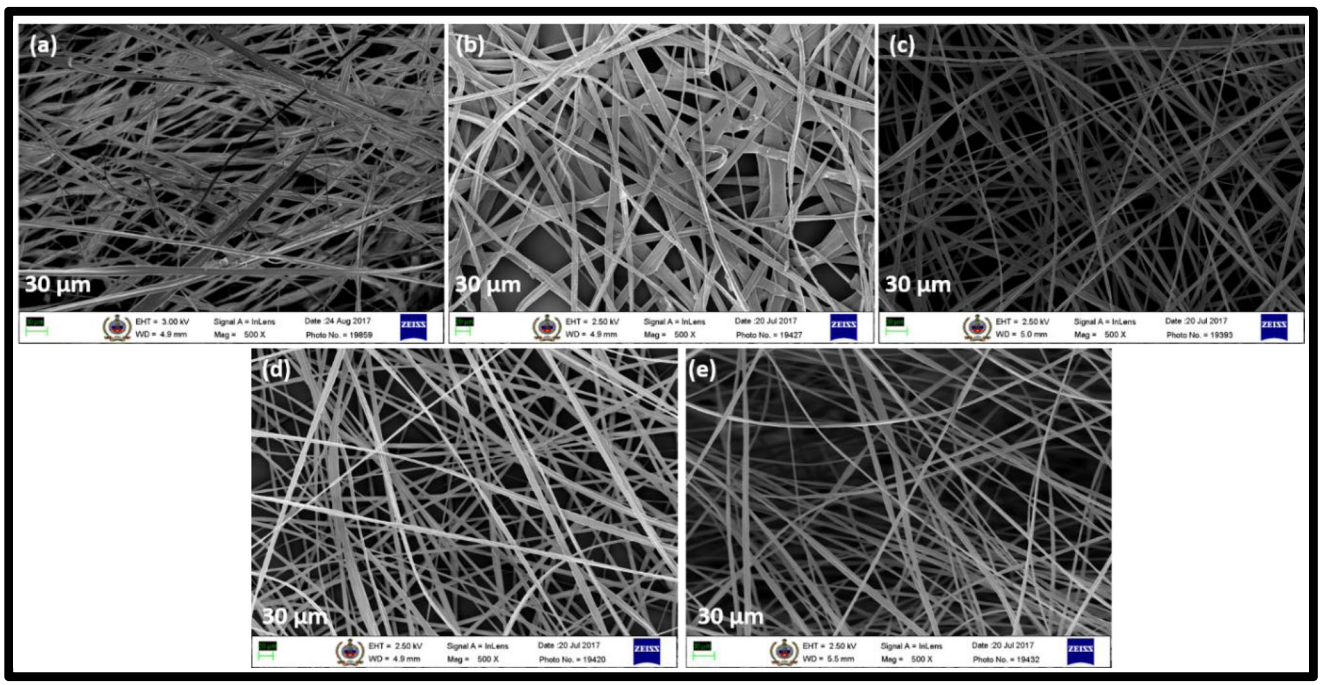

Fig. 4 FESEM micrographs of micro-fibers captured at 500X magnification of PHD/ABS (**a**) Neat ABS, (**b**) 0.1 wt% PHD, (**c**) 0.2 wt% PHD, (**d**) 0.3 wt% PHD, (**e**) 0.4 wt% PHD

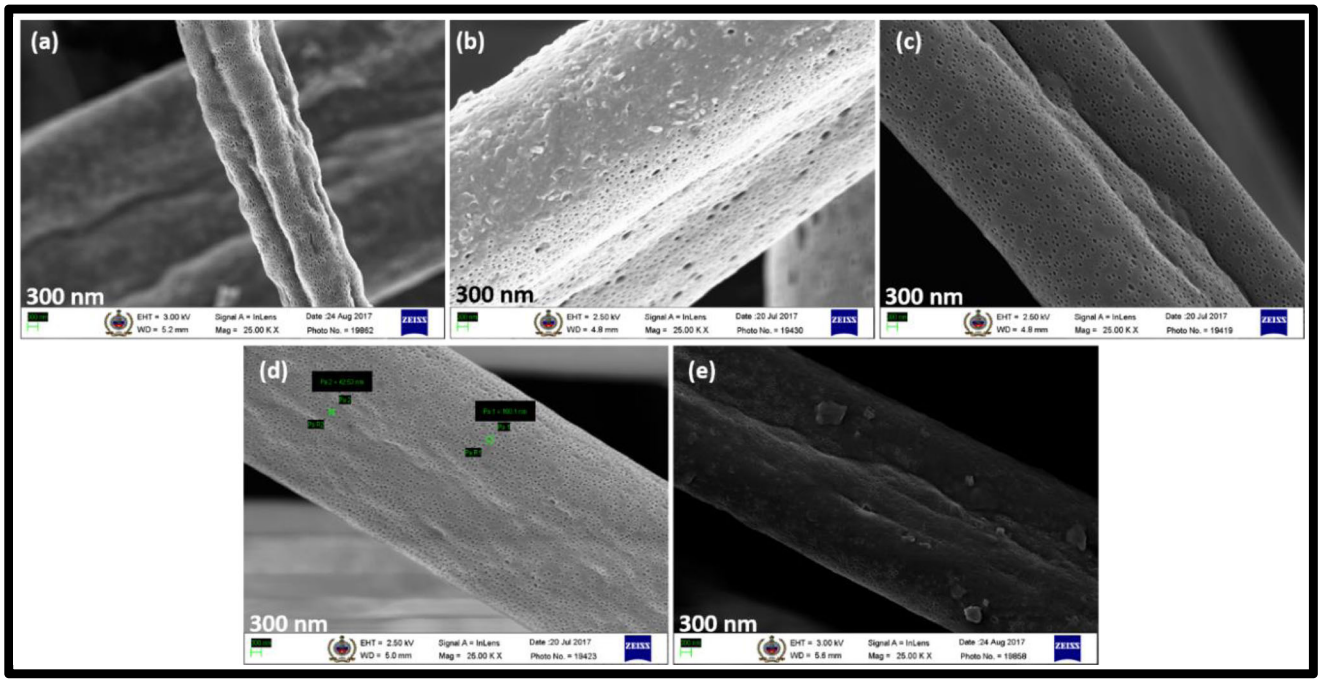

Fig. 5 FESEM micrographs of single micro-fibers PHD/ABS (**a**) Pristine ABS, (**b**) 0.1 wt% PHD, (**c**) 0.2 wt% PHD, (**d**) 0.3 wt% PHD, (**e**) 0.4 wt% PHD

contact angle analysis reveals that the hydrophobicity of PHD/ABS micro-fibers enhances with an increasing concentration of the PHD polymer.

For scrutinizing the wettability behavior of the materials owing to its hierarchical surface roughness, several wetting regimes have been established including the Wenzel and Cassie-Baxter [55, 56]. Considering the Wenzel's wetting regime, roughness on the homogeneous surface acts as the driving force for imparting the hydrophobicity to the material, thereby facilitating the transport of liquid e.g. water, over its surface, as explained in Fig. 8a. The Wenzel wetting regime can be explained using the following equation [55]:

$$\cos\theta_a = r.\cos\theta \quad (1)$$

Where, θ_a = homogenious rough surface contact angle , r = the surface roughness factor , which is a ratio of the authentic and the projected surface area and, θ = Young ' s contact angle [55].

The surface of nonwoven PHD/ABS micro-fibers can be considered as a heterogeneous hierarchical roughness, owing to its porous nature and rough micro-fiber surface, as the micro-fibers collected on the Aluminum sheets were randomly oriented. The wettability behavior of the hydrophobic materials exhibiting heterogeneous rough surface can be explained via Cassie-Baxter's wetting regime, wherein the hydrophobic feature probably attributes to the surface roughness/nanoneedles exerted capillary forces (Fig. 8b), and is given by the following equation [14, 15, 52, 56]:

$$cos\theta_x = F_1 cos\theta_a - F_2 \quad (2)$$

Where,

θ_x	apparent contact angle,
θ_a	contact angle of phase 1 and.
$F_1$and	surface fractions for phase 1 and 2, respectively
F_2	[14, 56].

Droplets of water rests onto the surface of the PHD/ABS micro-fibers owing to its porous nature and hierarchical textured surface morphology, while the low moisture absorption property of the PHD further enhances the hydrophobic characteristics of the developed micro-fibers.

Considering the important parameter of surface roughness, as described in Wenzel, and Cassie-Baxter theories, which help in improving the non-wetting behaviour of the surface, the FE-SEM micrographs of the Pure PHD, and PHD-ABS microfibers were analyzed using ImageJ software (version~1.52p) (Fig. 9).

The manifesting surface roughness has been clearly observed in the micrographs shown in Fig. 8, thereby, confirming the theoretical assumptions predicted in the Wenzel, and Cassie-Baxter theories [55, 56].

In order to evaluate the physical wetting properties of the developed microfibers, its work of adhesion, spreading coefficient, and wetting behaviour with respect to wt% loading of PHD were calculated [57]. The literature study states that if the calculated spreading coefficient is positive, then the surface exhibits spreadability towards liquid e.g. hydrophilicity

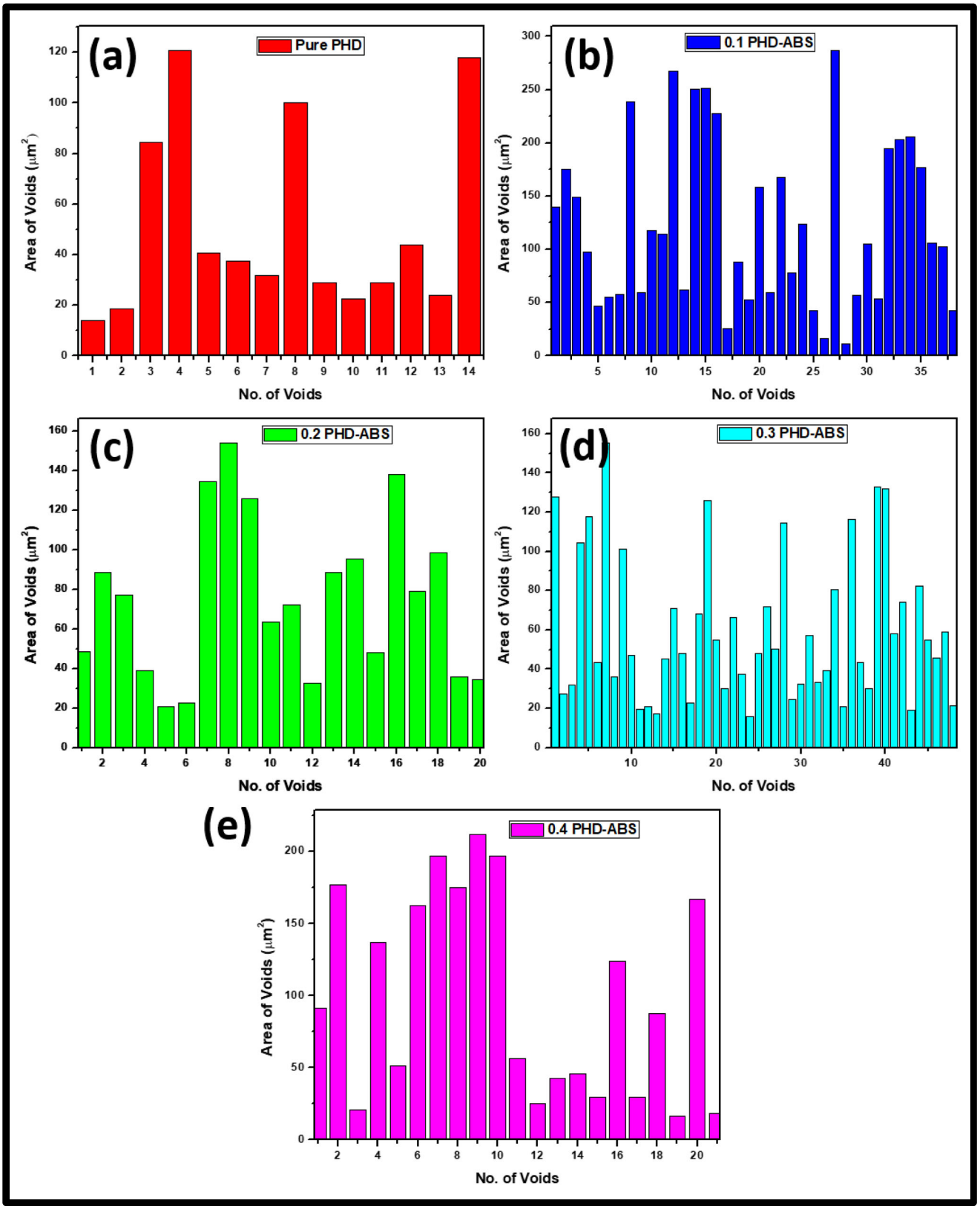

Fig. 6 Histograms of pore sizes in developed microfibers for (**a**) Pure PHD, (**b**) 0.1 wt% PHD-ABS, (**c**) 0.2 wt% PHD-ABS, (**d**) 0.3 wt% PHD-ABS, and (**e**) 0.4 wt% PHD-ABS

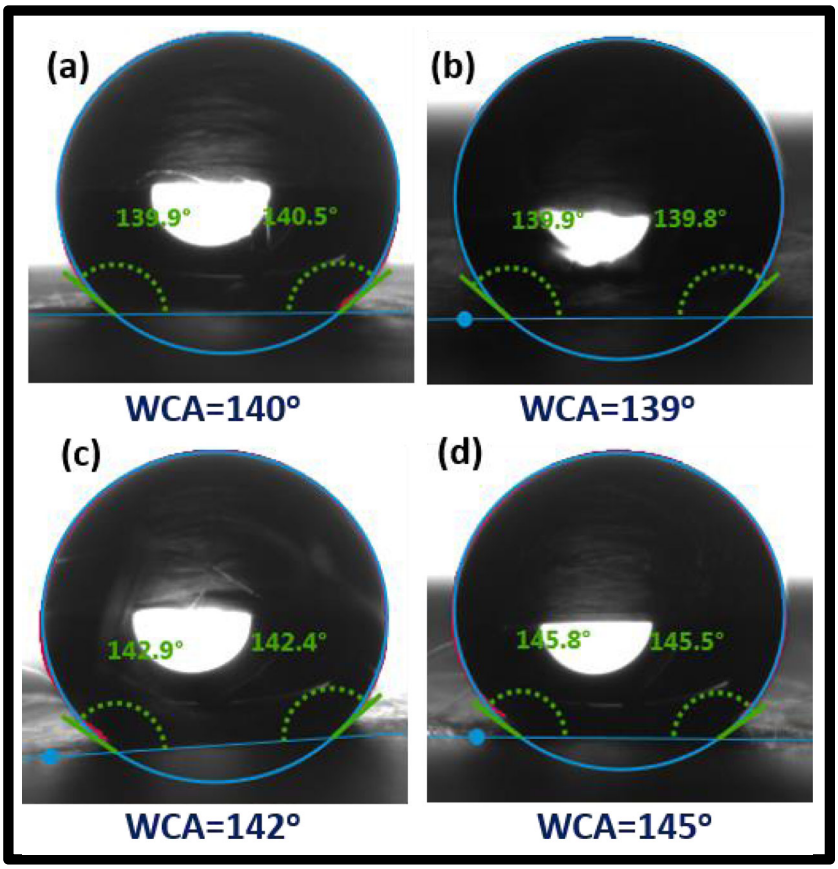

Fig. 7 Static water contact angles of micro-fibers (**a**) Pristine ABS (**b**) 0.2 *w*/w% PHD (**c**) 0.3 w/w% PHD (**d**) 0.4 w/w% PHD

towards water, and if the calculated value is negative, then the surface displays non-spreadability e.g. non-wetting hydrophobic nature towards water [57].

The work of adhesion, and spreading coefficients for the developed microfibers, were calculated using following equations [57–59]:

$$W_{12} = \sigma_l\,(1 + cos\theta) \tag{3}$$

Where,

$\boldsymbol{W_{12}}$ work of adhesion for surface at liquid-solid interface,
$\boldsymbol{\sigma_l}$ surface tension of the liquid,
$\boldsymbol{\theta}$ contact of the liquid with solid surface.

$$W_{11} = 2\sigma_l \tag{4}$$

Where,

$\boldsymbol{W_{11}}$ work of cohesion,
$\boldsymbol{\sigma_l}$ surface tension of the liquid.

$$S = W_{12} - W_{11} \tag{5}$$

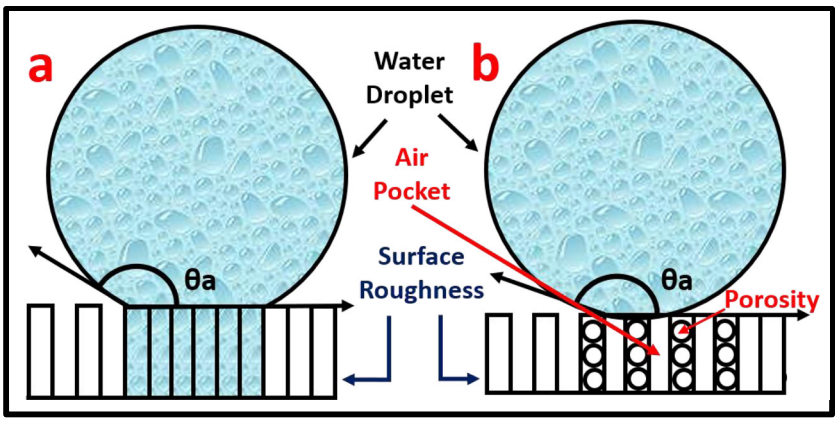

Fig. 8 (**a**) Wenzel Regime, (**b**) Cassie-Baxter Regime

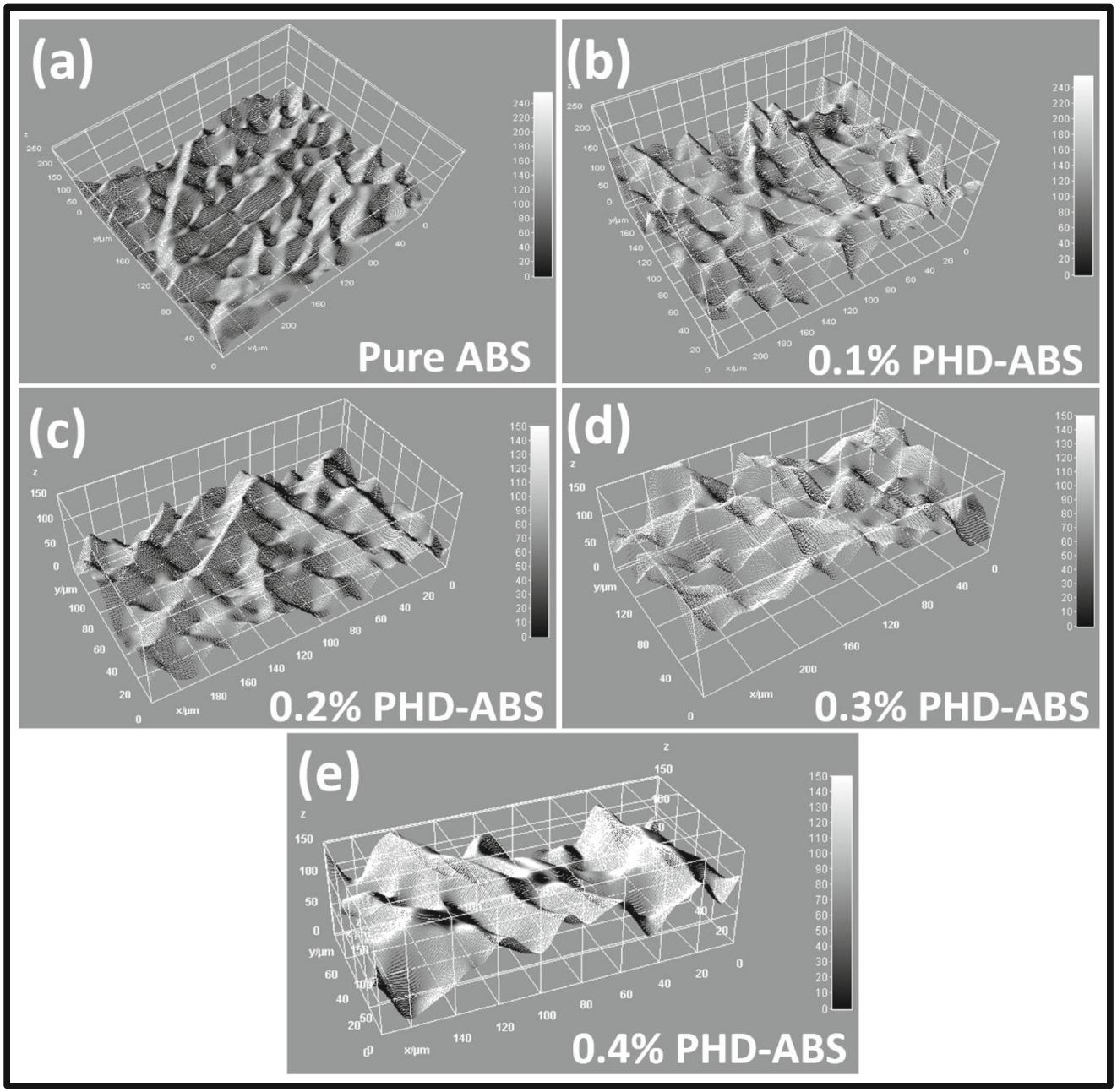

Fig. 9 Micrographs representing surface roughness on surface of the microfibers of (**a**) Pure ABS, (**b**) 0.1 wt% PHD-ABS, (**c**) 0.2 wt% PHD-ABS, (**c**) 0.3 wt% PHD-ABS, and (**d**) 0.4 wt% PHD-ABS

Where,

S spreading coefficient,
W_{12} work of adhesion,
W_{11} work of cohesion.

The work of adhesion for developed microfibers of Pure ABS, 0.2 wt% PHD-ABS, 0.3 wt% PHD-ABS, and 0.4 wt% PHD-ABS was found to be 0.0584 J/m^2, 0.12506 J/m^2, 0.0139 J/m^2, and 0.13714 J/m^2, respectively. The work of cohesion fore water (surface tension~72.8 mN/m) was found to be 0.1456 J/m^2.

The spreading coefficients for microfibers of Pure ABS, 0.2 wt% PHD-ABS, 0.3 wt% PHD-ABS, and 0.4 wt% PHD-ABS were found to be −0.08719 J/m^2, −0.02053 J/m^2, −0.13169 J/m^2, and − 0.00845 J/m^2, respectively. In present study, it is clearly observed that, the work of cohesion is larger than the work of adhesion, thereby, leading all spreading coefficients to be negative, which implies that the developed microfibers exhibit non-spreading i.e. hydrophobicity, towards water [57–59]. The plotted graphs representing the work of adhesion, spreading coefficients, and wetting behaviour

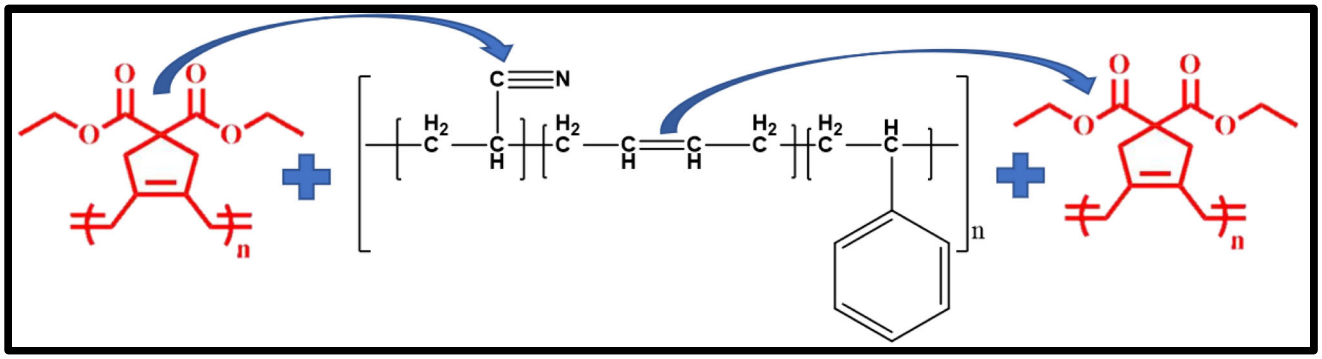

Fig. 10 Possible molecular interactions between PHD and ABS polymer

have been shown in Figure S5, in attached Supporting Information file.

Work of adhesion refers to the free energy difference between two defined states, the first of two phases which contact in equilibrium and the second phase being separate in equilibrium. The second state reveals the separation induced hydrophobic characteristic, which was observed in present study (Figure S5). This is described by analyzing the free energy difference, estimated by calculating the 'spreading coefficient'. Simon et al., have reported that the parameters of work adhesion and work cohesion and spreading coefficient, a negative value of these energies implies lack of spontaneous wetting, which indicates the hydrophobic nature exhibited by the surface [58]. This confirmed by the observed higher work adhesion value, which suggests that the large amount of energy is required to separate the water drops from the surface of the developed material [58, 59].

Jose et al. have reported the effect of free surface energy on the wetting behaviour of the surface, which states that, when the interfacial energy of the solid–vapour phase is lower, then its propensity for spreading to remove the interface is lower. In such circumstance, the material surface shows hydrophobic characteristic. Surface energy is linked with the interface of two phases, therefore, on reducing the free energy of the surface, the manifesting polymeric chains must interact with the additive surface i.e. in present study PHD in ABS, for achieving the hydrophobicity in the material [59]. This assumption is also supported by the increasing water contact angles on progressive wt% loading of PHD, and the negative spreading coefficients of the PHD-ABS microfibers.

In present study, the utilized PHD polymer exhibits maximum content of polar '-C-O-', and '-C=O' groups, whereas the ABS polymer exhibits functional '-CH-CN', and '-HC=CH-' groups. It is most likely that the functional groups present in ABS most possibly interact with '-C-O-', and '-C=O' groups present in PHD polymer. Further, these polar groups of PHD polymer help in repelling the water molecules (Fig. 10) [14, 52, 60].

Ice adhesion study

The Ice adhesion i.e. anti-icing, study of the developed PHD/ABS micro-fibers was accomplished by placing de-ionised water droplets of 8 µl volume (supercooled at -5 °C) on the pre-cooled surface of the micro-fibers. Further, the PHD/ABS micro-fibers with resting DI water droplets were subsequently placed in deep freezer system at a controlled temperature of -80 °C, for a period of 15 min.

Afterwards, the PHD/ABS micro-fibers with frozen water droplets were kept on the table, where immediately a pressurized airstream with a progressively increasing air-flow rate of 10 kPa per sec was supplied. The air-gun to PHD/ABS microfiber surface distance was maintained at length of 15 cm, and the air-gun to surface angle was kept at 45°. Immediately, after starting the pressurized air-stream, the frozen water droplets started to roll-off, and were completely removed from the PHD/ABS micro-fibers after few seconds as shown in Movie S1 (Supporting Information). Results of Ice adhesion study have been shown in Table 2.

Table 2 Ice adhesion study results

Microfiber Samples	Air Pressure	Frozen water droplet removal time
Pristine ABS micro--fibers	78 kPa	7 s
0.1 PHD/ABS micro-fibers	78 kPa	8 s
0.2 PHD/ABS micro-fibers	98 kPa	9.5 s
0.3 PHD/ABS micro-fibers	98 kPa	10 s
0.4 PHD/ABS micro-fibers	117 kPa	14 s

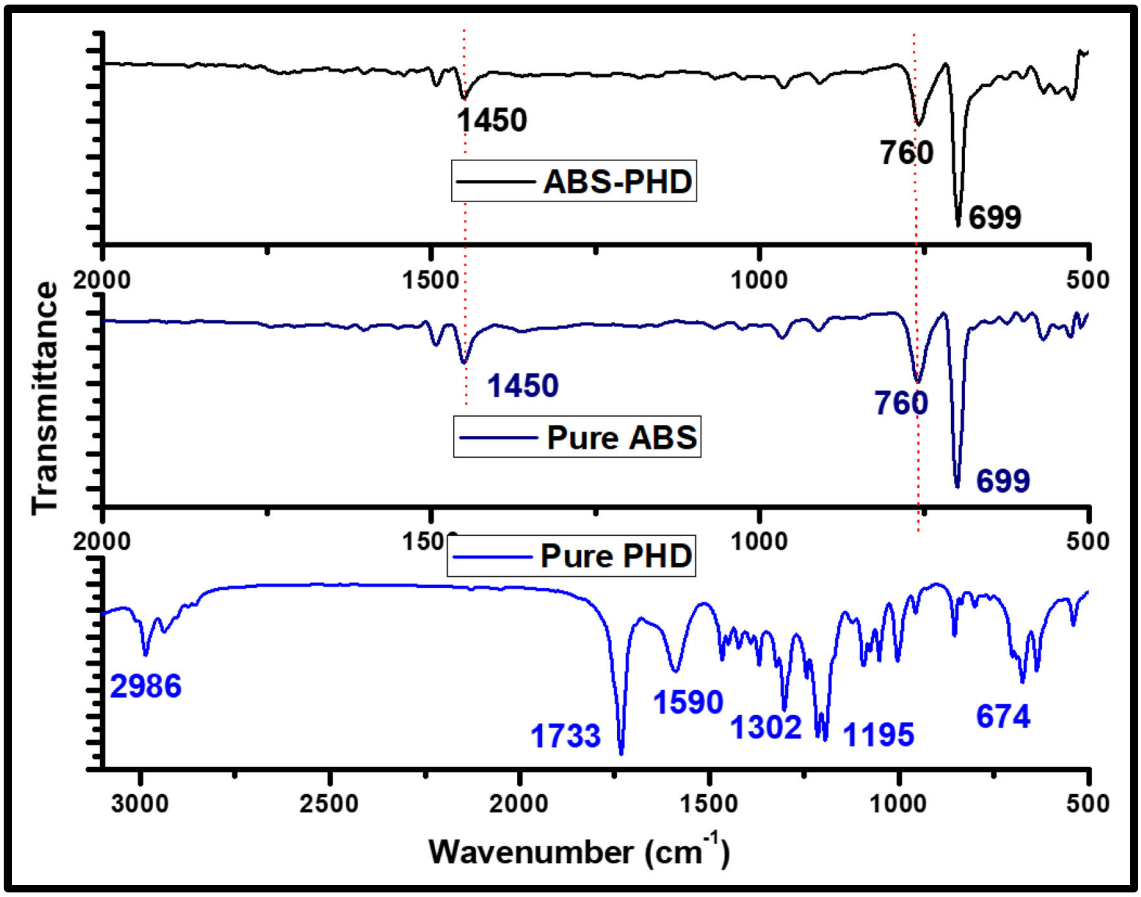

Fig. 11 FTIR study of Pure PHD, Pure ABS, and PHD-ABS microfibers

As shown in Table 1, the results reveal that, the pristine ABS & 0.1 wt% PHD/ABS micro-fibers require same air pressure (78 kPa), and has a water droplets removal time difference of 1 s, whereas 0.2 wt% PHD/ABS & 0.3 wt% PHD/ABS micro-fibers also require same air pressure (98 kPa) and water droplets removal time lag of 1.5 s. The 0.4 wt% PHD/ABS micro-fibers exhibit an air pressure of 117 kPa to remove the water droplets in 14 s. Pristine ABS micro-fibers required less air pressure (78 kPa) with a water droplet removal time (8 s) compared to other PHD/ABS micro-fiber samples. As the concentration of PHD increased in PHD/ABS micro-fibers, the respective required air pressure and water removal time also increased slightly. This enhancement in air pressure and water droplet removal time could be ascribed to Petal effect i.e. a superhydrophobic state with acting adhesive forces between nano−/micro-fiber surface & resting water droplets, and it is attributed to the impregnating Cassie wetting regime, where a roughness on the homogeneous surface acts as the driving force for conferring the hydrophobicity to the micro-fibers [7, 14]. Further, differences observed for the ice adhesion studies could also be attributed to Joule-Thomson cooling effect [61, 62]. This effect states that the change in temperature of a real gas/liquid (as compared to ideal gas) occurs, when the gas/liquid (when insulated for restricting the heat exchange with an environment) passes through a die/orifice/porous-plug [61–63]. Thus, considering the Joule-Thomson effect (due to utilization of compressed air in the current Ice adhesion study), it is possible that when air at low pressure comes in contact with environment it immediately gets warmer, and the air at high pressure takes time to get warmer, when it enters in the environment [61, 62]. Thus, the air stream generated by lower pressure drop will be warmer than that at the higher pressure, which could be attributed to slightly shorter removal time observed for frozen droplets [61, 62]. Increased droplet removal time could also be associated to different surface morphologies exhibited by PHD-ABS micro-fibers (Fig. 5). As the concentration of PHD increases in PHD-ABS blend microfibers, the respective heterogeneity occur on the blend surface. This surface heterogeneity due to increasing PHD concentration, probably causes the water droplets to permeate and fit into the generated nano/micro cavities (which occurs in Wenzel state). Thus, on supercooling, these frozen water droplets get mechanically interlocked in nano/micro cavities (also known as 'water droplet nucleation' due to heterogeneity on rough hydrophobic surfaces), thereby enhancing the adhesion between heterogenous micro-fiber surface and frozen water droplets [64, 65].

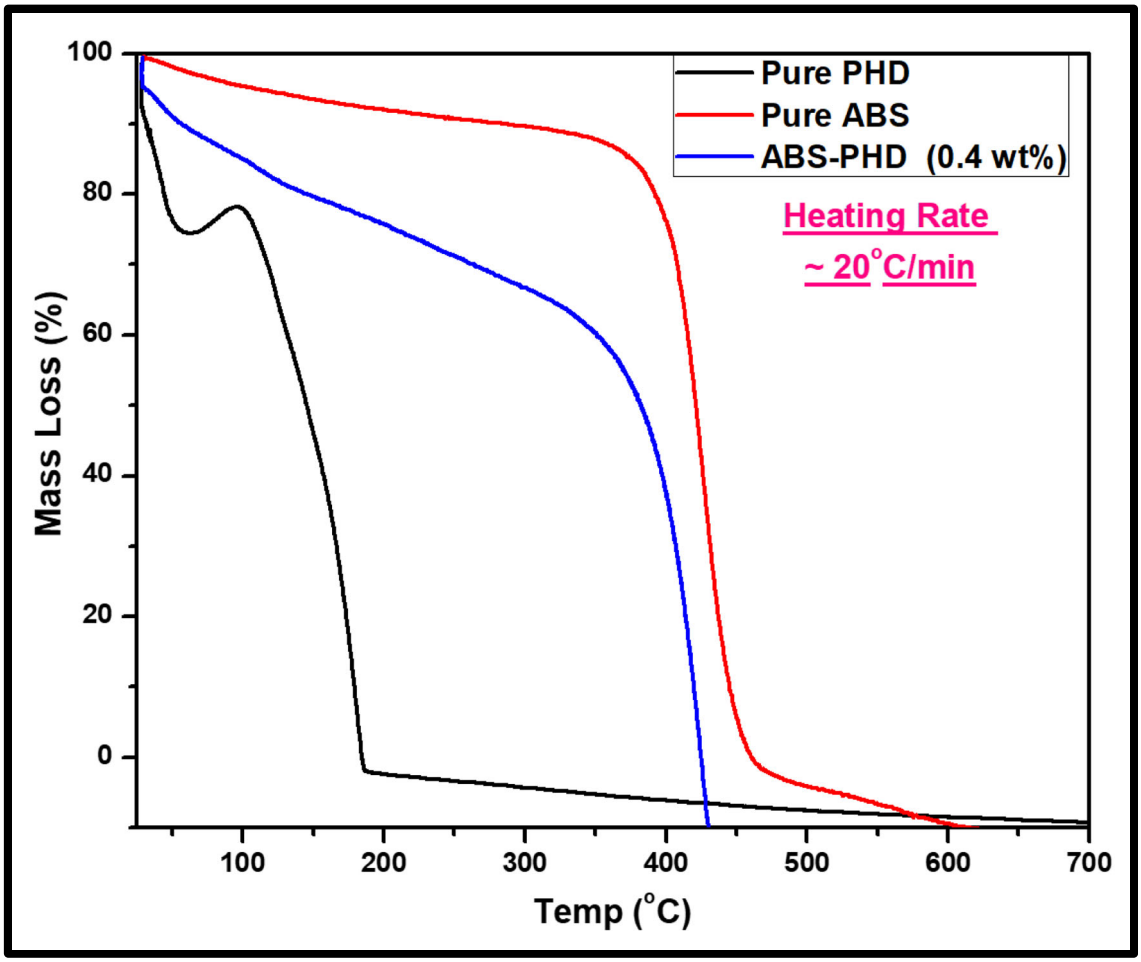

Fig. 12 TGA thermograms of Pure PHD, Pure ABS, and PHD-ABS blend

FTIR analysis

Fourier Transform Infrared Spectroscopy (FTIR) analysis was performed on Pure PHD, Pure ABS, and PHD-ABS microfibers, for determining the manifesting functional groups (Fig. 11). Study was performed using ATR-FTIR instrument (Bruker Inc., USA). FTIR plots of Pure ABS and PHD-ABS (0.4 wt/wt%) microfibers show characteristic peaks of ABS polymer, which is attributed to the well dispersion of PHD polymer during in-situ solution blending.

Pure ABS, and PHD-ABS microfibers show peaks at 1450 cm^{-1}, 760 cm^{-1}, and 699 cm^{-1}, which are attributed to 'C=C' stretch in mono substituted benzene ring i.e. styrene, 'C-H' bend in styrene, and '=C-H' bend in butadiene phase of ABS [66]. Further, typical characteristics peaks for Pure PHD were observed at 2986 cm^{-1}, 1733 cm^{-1}, 1590 cm^{-1}, 1302 cm^{-1}, 1195 cm^{-1}, and 674 cm^{-1}. Pure PHD peak at 2986 cm^{-1} corresponds to '-CH_2-' group, 1733 cm^{-1} corresponds to '-COO-' group, 1590 cm^{-1} corresponds to '-HC=CH-' group, whereas, peak at 1195 cm^{-1} corresponds to '-OCH_2-' group, thereby confirming its functional groups [42, 43, 49, 50].

Thermogravimetric analysis

Thermogravimetric analysis (TGA) was performed for analyzing the thermal stability of PHD-ABS microfibers. During TGA experiments, the heating rate was maintained at 20 °C/min, under inert atmosphere where Nitrogen gas was utilized at a flow rate of 20 ml/min. The results of TGA study have been represented in Fig. 12. TGA plots show that Pure ABS & PHD-ABS microfibers have thermal stability up to 350 °C, whereas the Pure un-crosslinked PHD polymer in gel form has showed low thermal stability, which thermally degraded within 200 °C [52, 67, 68]. The earlier thermal degradation of the Pure PHD polymer is attributed to the cross-linking, which occurs between 70 °C to 100 °C. The cross-linking in PHD is attributed to the manifesting '-O-C=O' group, and triple bonds [42, 44, 67–69]. During in-situ solution blending, PHD has well dispersed in ABS solution, thereby, giving the thermal stability i.e. around 350 °C, between Pure PHD, and Pure ABS, which is also evident from the TGA plots shown in Fig. 12.

Future Scope & Conclusion

Considering the hydrophobic nature, and thermal stability, PHD-ABS blend microfibers could be utilized for multifunctional applications like self-cleaning textiles & coatings, anti-biofouling & anti-corrosive surfaces, ice-phobic coatings, and oil-water separation. Mahalingam et al. have demonstrated a new pressure gyration based technique which can be utilized for the generation of nanofibers [70]. It is proposed that by utilizing pressure gyration technique, PHD/ABS micro-fibers can be produced in the form of sheath over core fibers, for producing the robust core-sheath nanofibers for above-targeted applications, further, the pristine PHD based core-sheath nanofibers can be utilized for potential bi-phasic drug delivery application [40, 70]. Pressurized gyration is an effective, simple and multipurpose technique, for producing nanofibers exhibiting controlled size and distribution, on mass scale at room temperature [70–72]. This technique involves a vessel which contains polymeric solution, which undergoes centrifugally acting force, where it facilitates formation of tailored nanofibers from dynamically flowing liquid via extrusion through orifices manifesting in the vessel [70–72]. Nanofibers generated by this technique, exhibit different morphologies based on speed of rotation of vessel, polymer solution concentration, applied pressure, and further, polymer exhibiting high molecular weight and orientation can yield mechanically strong nanofibers with highly active surface areas [70–72]. Thus, we have successfully fabricated a porous nonwoven hierarchically textured thermally stable PHD/ABS micro-fibers via in-situ solution blending by utilizing electrospinning technique. The developed PHD/ABS microfibers demonstrate hydrophobicity (WCA~145$^{o} \pm 5^{o}$), and possesses inherent hierarchical surface morphology as confirmed by the FESEM analysis. The PHD/ABS micro-fibers intrinsically possess a high thermal stability i.e. up to 300 °C. The miscibility of the PHD & ABS i.e. Chi parameter ($\chi_c = 7.88$) & free energy of mixing (4.67 kcal/mol), were evaluated using the molecular dynamics simulation analysis via Accelrys Materials Studio software, revealing the immiscible nature of the PHD and ABS homopolymers. The PHD/ABS engineered porous nonwoven micro-fibers also demonstrate a low ice adhesion ability, where it effectively removes the frozen water droplets in 8 s under an air pressure of 78 kPa. Considering the high thermal stability, the enhanced hydrophobicity, and the low ice adhesion ability, the developed PHD/ABS porous nonwoven micro-fibers can be efficiently used for the various multifunctional engineering applications involving hydrophobicity and high temperature applications.

Acknowledgements The authors are thankful to Dr. C. P. Ramanarayanan, Vice-Chancellor of DIAT (DU), Pune for motivation and support. The authors are also thankful to anonymous reviewers for their valuable suggestions, and comments, which helped in improving the quality of the manuscript.

References

1. Schlaich C, Wei Q, Haag R (2017) Mussel-inspired Polyglycerol coatings with controlled wettability: from Superhydrophilic to Superhydrophobic surface coatings. Langmuir 33:9508–9520. https://doi.org/10.1021/acs.langmuir.7b01291
2. Almohammadi H, Amirfazli A (2017) Understanding the drop impact on moving hydrophilic and hydrophobic surfaces. Soft Matter 13:2040–2053. https://doi.org/10.1039/C6SM02514E
3. Al-Azawi A, Latikka M, Jokinen V et al (2017) Friction and wetting transitions of magnetic droplets on micropillared Superhydrophobic surfaces. Small 13:1700860. https://doi.org/10.1002/smll.201700860
4. Gore PM, Balakrishnan S, Kandasubramanian B (2019) Superhydrophobic corrosion inhibtion polymer coatings. Superhydrophobic polymer coatings: fundamentals, design, fabrication, and applications1st edn. Elsevier, Amsterdam, pp 1–22
5. Xue C-H, Li Y-R, Zhang P, Ma JZ, Jia ST (2014) Washable and Wear-resistant Superhydrophobic surfaces with self-cleaning property by chemical etching of fibers and Hydrophobization. ACS Appl Mater Interfaces 6:10153–10161. https://doi.org/10.1021/am501371b
6. Liu D, Wang Q, Shen W, Wang D (2017) Self-cleaning antireflective coating with a hierarchical texture for light trapping in micromorph solar cells. J Mater Chem C 5:103–109. https://doi.org/10.1039/C6TC03152H
7. Gupta P, Kandasubramanian B (2017) Directional fluid gating by Janus membranes with heterogeneous wetting properties for selective oil–water separation. ACS Appl Mater Interfaces 9:19102–19113. https://doi.org/10.1021/acsami.7b03313
8. Sahoo BN, Balasubramanian K, Sucheendran M (2015) Thermally triggered transition of superhydrophobic characteristics of micro- and nanotextured multiscale rough surfaces. J Phys Chem C: 150610094322003. https://doi.org/10.1021/acs.jpcc.5b02917
9. Zhang P, Lin L, Zang D et al (2017) Designing bioinspired antibiofouling surfaces based on a Superwettability strategy. Small 13:1503334. https://doi.org/10.1002/smll.201503334
10. Gore PM, Naebe M, Wang X, Kandasubramanian B (2019) Progress in silk materials for integrated water treatments: fabrication, modification and applications. Chem Eng J 374:437–470. https://doi.org/10.1016/j.cej.2019.05.163
11. Gore PM, Khurana L, Siddique S, Panicker A, Kandasubramanian B (2018) Ion-imprinted electrospun nanofibers of chitosan/1-butyl-3-methylimidazolium tetrafluoroborate for the dynamic expulsion of thorium (IV) ions from mimicked effluents. Environ Sci Pollut Res 25:3320–3334. https://doi.org/10.1007/s11356-017-0618-6
12. Gore P, Khraisheh M, Kandasubramanian B (2018) Nanofibers of resorcinol–formaldehyde for effective adsorption of As (III) ions from mimicked effluents. Environ Sci Pollut Res 25:11729–11745. https://doi.org/10.1007/s11356-018-1304-z
13. Rajhans A, Gore PM, Siddique SK, Kandasubramanian B (2019) Ion-imprinted nanofibers of PVDF/1-butyl-3-methylimidazolium tetrafluoroborate for dynamic recovery of europium (III) ions from mimicked effluent. J Environ Cheml Eng 7:103068. https://doi.org/10.1016/j.jece.2019.103068
14. Gore PM, Kandasubramanian B (2018) Heterogeneous wettable cotton based superhydrophobic Janus biofabric engineered with PLA/functionalized-organoclay microfibers for efficient oil–water

separation. J Mater Chem A 6:7457–7479. https://doi.org/10.1039/C7TA11260B
15. Gore PM, Dhanshetty M, Kandasubramanian B (2016) Bionic creation of Nano-engineered Janus fabric for selective oil/organic solvent absorption. RSC Adv. https://doi.org/10.1039/C6RA24106A
16. Mishra P, Balasubramanian K (2014) Nanostructured microporous polymer composite imprinted with superhydrophobic camphor soot, for emphatic oil–water separation. RSC Adv 4:53291–53296. https://doi.org/10.1039/C4RA07410F
17. Arora R, Balasubramanian K (2014) Hierarchically porous PVDF/nano-SiC foam for distant oil-spill cleanups. RSC Adv 4:53761–53767. https://doi.org/10.1039/C4RA09245G
18. Onda T, Shibuichi S, Satoh N, Tsujii K (1996) Super-water-repellent fractal surfaces. Langmuir 12:2125–2127. https://doi.org/10.1021/la950418o
19. Bazin D, Faure C (2017) Superhydrophobic, highly adhesive arrays of copper hollow spheres produced by electro-colloidal lithography. Soft Matter 13:5500–5505. https://doi.org/10.1039/C7SM01256J
20. Zhuang A, Liao R, Dixon SC et al (2017) Transparent superhydrophobic PTFE films via one-step aerosol assisted chemical vapor deposition. RSC Adv 7:29275–29283. https://doi.org/10.1039/C7RA04116K
21. Yuan Z, Chen H, Tang J et al (2007) A novel preparation of polystyrene film with a superhydrophobic surface using a template method. J Phys D Appl Phys 40:3485–3489. https://doi.org/10.1088/0022-3727/40/11/033
22. Su X, Li H, Lai X, Zhang L, Wang J, Liao X, Zeng X (2017) Vapor–liquid sol–gel approach to fabricating highly durable and robust Superhydrophobic Polydimethylsiloxane@silica surface on polyester textile for oil–water separation. ACS Appl Mater Interfaces 9:28089–28099. https://doi.org/10.1021/acsami.7b08920
23. Qing Y, Hu C, Yang C, An K, Tang F, Tan J, Liu C (2017) Rough structure of Electrodeposition as a template for an Ultrarobust self-cleaning surface. ACS Appl Mater Interfaces 9:16571–16580. https://doi.org/10.1021/acsami.6b15745
24. Wu M, An N, Li Y, Sun J (2016) Layer-by-layer assembly of fluorine-free polyelectrolyte–surfactant complexes for the fabrication of self-healing Superhydrophobic films. Langmuir 32:12361–12369. https://doi.org/10.1021/acs.langmuir.6b02607
25. Hu Z, Berry RM, Pelton R, Cranston ED (2017) One-pot water-based hydrophobic surface modification of cellulose Nanocrystals using plant polyphenols. ACS Sustain Chem Eng 5:5018–5026. https://doi.org/10.1021/acssuschemeng.7b00415
26. Sahoo BN, Kandasubramanian B (2014) Photoluminescent carbon soot particles derived from controlled combustion of camphor for superhydrophobic applications. RSC Adv 4:11331. https://doi.org/10.1039/c3ra46193a
27. Tian X, Shaw S, Lind KR, Cademartiri L (2016) Thermal processing of silicones for Green, scalable, and healable Superhydrophobic coatings. Adv Mater 28:3677–3682. https://doi.org/10.1002/adma.201506446
28. Murdoch TJ, Willott JD, de Vos WM et al (2016) Influence of anion Hydrophilicity on the conformation of a hydrophobic weak polyelectrolyte brush. Macromolecules 49:9605–9617. https://doi.org/10.1021/acs.macromol.6b01897
29. Harvey BG, Guenthner AJ, Koontz TA et al (2016) Sustainable hydrophobic thermosetting resins and polycarbonates from turpentine. Green Chem 18:2416–2423. https://doi.org/10.1039/C5GC02893K
30. Chung C-Y, Warkiani ME, Mesgari S et al (2015) Thermoset polyester-based superhydrophobic microchannels for nanofluid heat transfer applications. In: Eggleton BJ, Palomba S (eds) Sydney. New South Wales, Australia, p 96680D
31. Cao W-T, Liu Y-J, Ma M-G, Zhu J-F (2017) Facile preparation of robust and superhydrophobic materials for self-cleaning and oil/water separation. Colloids Surf A Physicochem Eng Asp 529:18–25. https://doi.org/10.1016/j.colsurfa.2017.05.064
32. Söz CK, Yilgör E, Yilgör I (2016) Simple processes for the preparation of superhydrophobic polymer surfaces. Polymer 99:580–593. https://doi.org/10.1016/j.polymer.2016.07.051
33. Haselwander TFA, Heitz W, Krügel SA, Wendorff JH (1996) Polynorbornene: synthesis, properties and simulations. Macromol Chem Phys 197:3435–3453. https://doi.org/10.1002/macp.1996.021971029
34. Shang Y, Si Y, Raza A et al (2012) An in situ polymerization approach for the synthesis of superhydrophobic and superoleophilic nanofibrous membranes for oil–water separation. Nanoscale 4:7847. https://doi.org/10.1039/c2nr33063f
35. Sung G, Choi M-C, Nagappan S, Lee WK, Han M, Ha CS (2013) Polynorbornene/fluorosilica hybrids for hydrophobic and oleophobic coatings. Polym Bull 70:619–630. https://doi.org/10.1007/s00289-012-0882-z
36. Ruffoni A, Cavanna MV, Argentiere S et al (2016) Aqueous self-assembly of short hydrophobic peptides containing norbornene amino acid into supramolecular structures with spherical shape. RSC Adv 6:90754–90759. https://doi.org/10.1039/C6RA17116H
37. Grove NR, Kohl PA, Bidstrup Allen SA et al (1999) Functionalized polynorbornene dielectric polymers: adhesion and mechanical properties. J Polym Sci B Polym Phys 37:3003–3010. https://doi.org/10.1002/(SICI)1099-0488(19991101)37:21<3003::AID-POLB10>3.0.CO;2-T
38. Janiak C, Lassahn PG (2001) The vinyl Homopolymerization of Norbornene. Macromol Rapid Commun 22:479–493. https://doi.org/10.1002/1521-3927(20010401)22:7<479::AID-MARC479>3.0.CO;2-C
39. Maier G (2001) Low dielectric constant polymers for microelectronics. Prog Polym Sci 26:3–65. https://doi.org/10.1016/S0079-6700(00)00043-5
40. Rao NV, Mane SR, Kishore A, Das Sarma J, Shunmugam R (2012) Norbornene derived doxorubicin copolymers as drug carriers with pH responsive Hydrazone linker. Biomacromolecules 13:221–230. https://doi.org/10.1021/bm201478k
41. Bhattacharya S, Sarkar S, Shunmugam R (2013) Unique norbornene polymer based "in-field" sensor for As(iii). J Mater Chem A 1:8398. https://doi.org/10.1039/c3ta11587a
42. Sarkar S, Shunmugam R (2014) Polynorbornene derived 8-hydroxyquinoline paper strips for ultrasensitive chemical nerve agent surrogate sensing. Chem Commun 50:8511–8513. https://doi.org/10.1039/C4CC03361B
43. Mukherjee M, Ganivada MN, Venu P et al (2016) Unique nanotubes from polynorbornene derived graphene sheets. RSC Adv 6:40691–40697. https://doi.org/10.1039/C6RA05840J
44. Mane SR, Sarkar SNVR et al (2015) An efficient method to prepare a new class of regioregular graft copolymer via a click chemistry approach. RSC Adv 5:74159–74161. https://doi.org/10.1039/C5RA12510C
45. Fujiwara M, Shirato Y, Owari H et al (2007) Novel optical/electrical printed circuit board with Polynorbornene optical waveguide. Jpn J Appl Phys 46:2395–2400. https://doi.org/10.1143/JJAP.46.2395
46. Cao K, Siepermann CP, Yang M et al (2013) Reactive aramid nanostructures as high-performance polymeric building blocks for advanced composites. Adv Funct Mater 23:2072–2080. https://doi.org/10.1002/adfm.201202466
47. Joseph PJ, Kelleher HA, Allen SAB, Kohl PA (2005) Improved fabrication of micro air-channels by incorporation of a structural barrier. J Micromech Microeng 15:35–42. https://doi.org/10.1088/0960-1317/15/1/006
48. Hess-Dunning AE, Smith RL, Zorman CA (2014) Development of polynorbornene as a structural material for microfluidics and flexible BioMEMS. J Appl Polym Sci 131. https://doi.org/10.1002/app.40969

49. Magisetty R, Kumar P, Gore PM et al (2019) Electronic properties of poly(1,6-heptadiynes) electrospun fibrous non-woven mat. Mater Chem Phys 223:343–352. https://doi.org/10.1016/j.matchemphys.2018.11.020
50. Magisetty R, Kumar P, Kumar V, Shukla A, Kandasubramanian B, Shunmugam R (2018) NiFe2O4/poly(1,6-heptadiyne) Nanocomposite energy-storage device for electrical and electronic applications. ACS Omega 3:15256–15266. https://doi.org/10.1021/acsomega.8b02306
51. Huang Z-M, Zhang Y-Z, Kotaki M, Ramakrishna S (2003) A review on polymer nanofibers by electrospinning and their applications in nanocomposites. Compos Sci Technol 63:2223–2253. https://doi.org/10.1016/S0266-3538(03)00178-7
52. Gore PM, Zachariah S, Gupta P, K. B (2016) Multifunctional nano-engineered and bio-mimicking smart superhydrophobic reticulated ABS/fumed silica composite thin films with heat-sinking applications. RSC Adv 6:105180–105191. https://doi.org/10.1039/C6RA16781K
53. Khurana L, Balasubramanian K (2016) Adsorption potency of imprinted starch/PVA polymers confined ionic liquid with molecular simulation framework. J Environ Cheml Eng 4:2147–2154. https://doi.org/10.1016/j.jece.2016.03.032
54. Yadav R, Naebe M, Wang X, Kandasubramanian B (2016) Temperature assisted in-situ small angle X-ray scattering analysis of Ph-POSS/PC polymer nanocomposite. Sci Rep 6:6–9. https://doi.org/10.1038/srep29917
55. Wenzel RN (1936) Resistance of solid surfaces to wetting by water. Ind Eng Chem 28:988–994. https://doi.org/10.1021/ie50320a024
56. Cassie ABD, Baxter S (1944) Wettability of porous surfaces. Trans Faraday Soc 40:546. https://doi.org/10.1039/tf9444000546
57. Packham DE (1996) Work of adhesion: contact angles and contact mechanics. Int J Adhes Adhes 16:121–128. https://doi.org/10.1016/0143-7496(95)00034-8
58. Simon SM, Chandran A, George G, Sajna MS, Valparambil P, Kumi-Barmiah E, Jose G, Biju PR, Joseph C, Unnikrishnan NV (2018) Development of thick Superhydrophilic TiO2–ZrO2 transparent coatings realized through the inclusion of poly(methyl methacrylate) and Pluronic-F127. ACS Omega 3:14924–14932. https://doi.org/10.1021/acsomega.8b01940
59. Jose JP, Abraham J, Maria HJ et al (2016) Contact angle studies in XLPE hybrid Nanocomposites with inorganic Nanofillers. Macromol Symp 366:66–78. https://doi.org/10.1002/masy.201650048
60. Gore PM, Purushothaman A, Naebe M et al (2019) Nanotechnology for oil-water separation. In: advanced research in Nanosciences for water technology1st edn. Springer Science+Business Media, New York
61. Perry RH, Green DW, Maloney JO (1984) Perry's chemical engineers' handbook6th edn. McGraw-Hill, New York
62. Roy BN (2002) Fundamentals of classical and statistical thermodynamics. Wiley, West Sussex
63. Edmister WC, Lee BI (1984) Applied hydrocarbon thermodynamics2nd edn. Gulf Pub. Co, Houston
64. Wei C, Jin B, Zhang Q et al (2018) Anti-icing performance of super-wetting surfaces from icing-resistance to ice-phobic aspects: robust hydrophobic or slippery surfaces. J Alloys Compd 765:721–730. https://doi.org/10.1016/j.jallcom.2018.06.041
65. Elsharkawy M, Tortorella D, Kapatral S, Megaridis CM (2016) Combating frosting with joule-heated liquid-infused Superhydrophobic coatings. Langmuir 32:4278–4288. https://doi.org/10.1021/acs.langmuir.6b00064
66. Kuptsov AH, Zhizhin GN (1998) Handbook of fourier transform Raman and infrared spectra of polymers. Elsevier, Amsterdam, New York
67. Jeon S, Shim C, Cho CS et al (2000) Catalytic cyclopolymerization and copolymerization of 1,6-heptadiynes by Mo(CO)6. J Polym Sci A Polym Chem 38:2663–2670. https://doi.org/10.1002/1099-0518(20000801)38:15<2663::AID-POLA50>3.0.CO;2-6
68. Song W, Han H, Liao X et al (2014) Metathesis Cyclopolymerization of Imidazolium-functionalized 1,6-Heptadiyne toward Polyacetylene Ionomer. Macromolecules 47:6181–6188. https://doi.org/10.1021/ma501217b
69. Ganivada MN, Kumar P, Shunmugam R (2015) A unique polymeric gel by thiol–alkyne click chemistry. RSC Adv 5:50001–50004. https://doi.org/10.1039/C5RA06339F
70. Mahalingam S, Homer-Vanniasinkam S, Edirisinghe M (2019) Novel pressurised gyration device for making core-sheath polymer fibres. Mater Des 178:107846. https://doi.org/10.1016/j.matdes.2019.107846
71. Heseltine PL, Ahmed J, Edirisinghe M (2018) Developments in pressurized gyration for the mass production of polymeric fibers. Macromol Mater Eng 303:1800218. https://doi.org/10.1002/mame.201800218
72. Hong X, Mahalingam S, Edirisinghe M (2017) Simultaneous application of pressure-infusion-gyration to generate polymeric Nanofibers. Macromol Mater Eng 302:1600564. https://doi.org/10.1002/mame.201600564